Guidance, Navigation, and Control for Agile Small Spacecraft with Articulating Solar Arrays

Robert D. Magner, Niels Roth, Brad Cotten, Robert E. Zee
Space Flight Laboratory, University of Toronto Institute for Aerospace Studies
4925 Dufferin Street, Toronto, Ontario, Canada, M3H 5T6
rmagner@utias-sfl.net

ABSTRACT

Payload operations for small satellites are often impacted by the need to allocate time for modifying the attitude to perform power generation or orbit maneuvering. A typical small satellite design would consist of a single rigid body with body-mounted solar cells, making the power generation subject to the spacecraft's attitude. Often to achieve the high power generation that is required to enable the payload function, the attitude must be specifically set to maximize the solar cell area facing the Sun, which typically means diverting it from an attitude that is useful for payload operations for some period of time. At the scale of modern global constellations, these downtimes in the payload operation schedule can greatly reduce the overall capability of the system. By including deployable, articulating solar arrays in the design of small spacecraft, array pointing can be decoupled from the main payload pointing operations. With these pieces decoupled, payload operations can proceed uninterrupted while the articulating arrays ensure sufficient power generation. In this paper, the dynamic equations of the multibody system are derived, and guidance, navigation, and control (GNC) considerations are presented for achieving decoupled attitude and articulation objectives. Results from simulation of a sample mission show that agile target tracking attitude maneuvers can be performed together with array solar tracking with negligible impact on overall payload pointing performance.

I. Introduction

A limiting factor in any small satellite mission design is the amount of power that can be generated to enable the spacecraft's operations. Payload operations scheduling is often constrained by the need to periodically modify the attitude to perform dedicated Sun tracking operations for power generation. This is because small satellites are often designed with a fixed topology, which generally means that there are certain attitudes that are more favourable for power generation due to the number of solar cells that are pointed at the Sun, and these Sun-pointing attitudes are not generally compatible with more dynamic attitude trajectories needed for pointing the body-fixed payloads at Earth targets. These fixed topologies are favorable from a conventional small satellite design standpoint because they reduce the number of moving parts and thus, the potential failure points. For example, a science mission with a low payload duty cycle may opt for such a design as it can afford to spend large periods of its operations schedule focusing on power generation.

With the rise of the commercial small satellite industry, missions are being pursued with increasingly demanding operational profiles. Current and upcoming constellations aim to establish global communications networks, or to perform Earth observation with rapid revisit times. To achieve these goals, higher payload duty cycles are required for each spacecraft in the constellation. The conservative approach of relying on fixed spacecraft topologies with body fixed solar cells will not work when the mission cannot afford to allocate large fractions of the orbit to power generation. The approach then is to use a variable topology; articulating solar arrays can be made to track the Sun while the payload fixed to the main body tracks its target, to maximize power generation continuously.

The dynamics and control of multibody systems has been well studied for spacecraft and robotics applications. The use of *Natural Orthogonal Complement* (NOC) methodologies for reducing the multibody equations of motion into the joint space was initiated by Angeles and Lee [1], then later expanded on by Angeles and Ma [2] and Saha [3] [4]. These methodologies were applied to a space context by Virgili-Llop *et al.* [5] who released an open-source software toolkit for simulating spacecraft with attached robotic arms based on NOC dynamics. Attitude and shape control (i.e., articulation) of a spacecraft with reaction wheels has been addressed by Rui *et al.* [6], who focused on the underactuated case.

This paper focuses on the development of multibody models and guidance, navigation, and control (GNC) techniques that employ maximal reuse of heritage software systems for single body spacecraft. The heritage Space Flight Laboratory (SFL) attitude determination

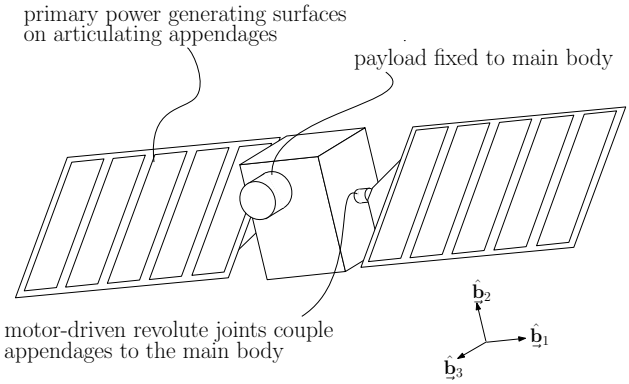

Fig. 1: Depiction of sample spacecraft using articulating solar arrays to enable a high-powered payload

and control system (ADCS) is leveraged for primary GNC of the spacecraft's main payload-carrying body, whereas new systems are added that provide articulation GNC for the appendages, and feed relevant updates back into the main ADCS for compensation due to multibody couplings.

Sample Mission

In this paper a generic mission concept is defined for the purpose of demonstrating the technology. The sample mission employs SFL's DEFIANT platform [7]. The spacecraft's primary operations consist of tracking Earth-fixed targets with a payload fixed to the main body (for example an imager or an antenna). Two deployable and articulating solar array appendages are coupled to the main body via stepper motor-driven revolute joints. The simple mechanical configuration has the joint axes orthogonal to the payload axis; as is shown in the depiction in Figure 1, the joint axes both point along the body X-axis, whereas the payload points along the body Z-axis. On the appendage side, the solar array's primary power generating surface is again orthogonal to the joint axis. While the main body attitude is governed to achieve the payload target tracking objectives, the articulation of the appendages will aim to maximize power generation.

II. Natural Orthogonal Complement Dynamic Model

For a system of n rigid bodies, the dynamics of each body i can be modelled with the Newton-Euler equations, expressed in its own body fixed frame:

$$\mathbf{I}_\mathrm{i}\dot{\boldsymbol{\omega}}_\mathrm{i} + \boldsymbol{\omega}_\mathrm{i}^{\times}\mathbf{I}_\mathrm{i}\boldsymbol{\omega}_\mathrm{i} = \boldsymbol{\tau}_\mathrm{i} \tag{1a}$$

$$m_i\dot{\mathbf{v}}_\mathrm{i} = \mathbf{f}_\mathrm{i} \tag{1b}$$

Where $\mathbf{I}_\mathrm{i}$ is the body's moment of inertia about its center of mass, m_i is its mass, $\mathbf{v}_\mathrm{i}$ and $\boldsymbol{\omega}_\mathrm{i}$ are the translational and angular velocities, respectively, and $\mathbf{f}_\mathrm{i}$ and $\boldsymbol{\tau}_\mathrm{i}$ are the forces and torques about the center of mass, respectively. Note that Eqn. (1) gives a total of $6n$ equations for the n-body system. The n-body systems that are considered here, however, are kinematic chains having m degrees of freedom, where in general $m < 6n$ due to joint coupling between adjacent bodies. For the case of a rotational joint connecting body i with body $i+1$, the bodies can rotate with respect to each other about the joint axis, but are constrained in the transverse axes.

For the purpose of computing the system's motion over time, we are primarily concerned with the *forward dynamics*, i.e., solving for the accelerations based on pre-computed forces and torques. Forces and torques from actuation and external disturbances can be readily computed using models of the disturbing environment and the actuator behaviour given an input control signal. On the other hand, the constraint forces and torques are unknowns, without already having knowledge of the *inverse dynamics* of the system.

We circumvent this issue by reducing the system using the Natural Orthogonal Complement (NOC). This formulation converts the $6n$ equations of motion expressed in the *operational space* (i.e., the combined Cartesian state space of all bodies) into an m-dimensional system of equations to fully model the *joint space* forward dynamics.

Unconstrained Operational Space Newton-Euler Equations

For ease of manipulation, the Newton-Euler equations (Eqn. 1) are reformulated into a more compact expression. To start, the robotic *twist*, $\mathbf{t}$, and *wrench*, $\mathbf{w}$ are defined as:

$$\mathbf{t} = \left[\mathbf{t}_1^T, \ldots, \mathbf{t}_\mathrm{n}^T\right]^T \quad \text{where} \quad \mathbf{t}_\mathrm{i} = \begin{bmatrix}\boldsymbol{\omega}_\mathrm{i}\\ \mathbf{v}_\mathrm{i}\end{bmatrix} \tag{2}$$

$$\mathbf{w} = \left[\mathbf{w}_1^T, \ldots, \mathbf{w}_\mathrm{n}^T\right]^T \quad \text{where} \quad \mathbf{w}_\mathrm{i} = \begin{bmatrix}\boldsymbol{\tau}_\mathrm{i}\\ \mathbf{f}_\mathrm{i}\end{bmatrix} \tag{3}$$

Then, the generalized mass matrix $\mathbf{M}$ and generalized angular velocity matrix $\mathbf{W}$ are given by:

$$\mathbf{M} = \mathrm{diag}\left[\mathbf{M}_1, \ldots, \mathbf{M}_\mathrm{n}\right], \text{ where } \mathbf{M}_\mathrm{i} = \begin{bmatrix}\mathbf{I}_\mathrm{i} & \mathbf{0}\\ \mathbf{0} & m_i\mathbf{1}_{3\mathrm{x}3}\end{bmatrix} \tag{4}$$

$$\mathbf{W} = \mathrm{diag}\left[\mathbf{W}_1, \ldots, \mathbf{W}_\mathrm{n}\right], \text{ where } \mathbf{W}_\mathrm{i} = \begin{bmatrix}\boldsymbol{\omega}_\mathrm{i}^{\times} & \mathbf{0}\\ \mathbf{0} & \mathbf{0}\end{bmatrix} \tag{5}$$

Where $\mathbf{1}_\mathrm{mxm}$ is the m-by-m identity matrix. Using the above definitions the operational space dynamics for the entire system are expressed as:

$$\mathbf{M}\dot{\mathbf{t}} + \mathbf{W}\mathbf{M}\mathbf{t} = \mathbf{w} \tag{6}$$

Kinematic Constraints in the Case of Two Rotating Appendages

The multibody system that this paper will focus on consists of three bodies: the main spacecraft body, and two solar arrays. The main spacecraft body is a *floating base* which means that it is a base body that is not rigidly fixed to an inertial frame. The two array appendages are each coupled to the main spacecraft with revolute joints. In the single body spacecraft attitude problem the motion is solved by integrating a forward-dynamics expression of Eqn. (1), then translational position can be solved through simple integration of the velocity whereas the attitude can be solved integrating the quaternion kinematics:

$$\dot{\mathbf{q}}_{\text{bi}} = \frac{1}{2}\begin{bmatrix} \eta\boldsymbol{\omega} - \boldsymbol{\omega}^{\times}\boldsymbol{\epsilon} \\ -\boldsymbol{\omega}^{T}\boldsymbol{\epsilon} \end{bmatrix} \tag{7}$$

Where $\mathbf{q}_{\text{bi}} = \begin{bmatrix}\boldsymbol{\epsilon}^T & \eta\end{bmatrix}^T$ is the inertial-to-body quaternion, and the Euler's parameters $\boldsymbol{\epsilon} = \boldsymbol{a}\sin(\frac{\phi}{2}), \quad \eta = \cos(\frac{\phi}{2})$ describe the Eigen-axis rotation of angle ϕ about axis $\boldsymbol{a}$ [8].

It would be possible to assign this representation to each of the three bodies, where there would then be 9 rotational and 9 translational velocities, then 9 translational center of mass positions and 12 total quaternion elements. As mentioned previously, the problem that is encountered here is in the calculation of the forward dynamics the constraint forces and torques are unknown, as they depend on the inverse dynamics of the next linked body. Instead, the constraints that the couplings place on the kinematics are invoked to reduce the dynamic equations. Letting the subscript 0 refer to the main body/floating base, then 1 and 2 refer to the two respective bodies coupled to the base via revolute joints, the following relations are found (note that the first two equalities are redundant, but are kept track of for the coming manipulations):

$$\begin{aligned}
\boldsymbol{\omega}_0 &= \boldsymbol{\omega}_0 \\
\mathbf{v}_{0,\text{i}} &= \mathbf{v}_{0,\text{i}} \\
\boldsymbol{\omega}_1 &= \boldsymbol{\omega}_0 + \mathbf{e}_1\dot{\theta}_1 \\
\mathbf{v}_{1,\text{i}} &= \mathbf{v}_{0,\text{i}} + \mathbf{e}_{1,\text{i}}^{\times}\mathbf{r}_{1,\text{i}}\dot{\theta}_1 \\
\boldsymbol{\omega}_2 &= \boldsymbol{\omega}_0 + \mathbf{e}_2\dot{\theta}_2 \\
\mathbf{v}_{2,\text{i}} &= \mathbf{v}_{0,\text{i}} + \mathbf{e}_{2,\text{i}}^{\times}\mathbf{r}_{2,\text{i}}\dot{\theta}_2
\end{aligned} \tag{8}$$

Where θ_j is the joint j rotation angle measured from some datum, $\mathbf{r}_{\text{j}}$ is the vector from $\mathbf{c}_0$ to $\mathbf{c}_{\text{j}}$, the center of masses of body 0 and body j, respectively, and $\mathbf{e}_{\text{j}}$ is the axis of rotation of the joint j. Note that $\boldsymbol{\omega}_{\text{j}}$ is expressed in the j body frame, and the bodies' frames are defined by convention such that the rotation axes are expressed the same between adjacent frames e.g. $\mathbf{e}_1 = \mathbf{e}_{1,0} = \mathbf{e}_{1,1}$. Furthermore, note here that when present, the second subscript denotes frame. When there is only one subscript, that subscript denotes the body to which that value pertains, and the vector is assumed to be expressed in that body's frame.

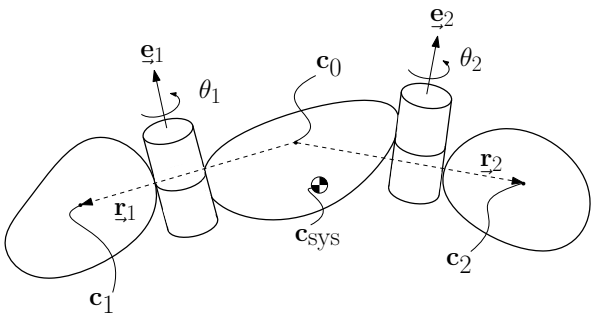

Fig. 2: Depiction of the 3 body system topology

In compact form, Eqn. (8) is expressed as:

$$\mathbf{t} = \mathbf{N}\dot{\boldsymbol{\Theta}} \tag{9}$$

Where:

$$\mathbf{N} = \begin{bmatrix} \mathbf{1}_{6\text{x}6} & \mathbf{0}_{6\text{x}1} & \mathbf{0}_{6\text{x}1} \\ \mathbf{L}_{3\text{x}6} & \mathbf{e}_1 & \mathbf{0}_{3\text{x}1} \\ \mathbf{L}_{3\text{x}6} & \mathbf{e}_{1,\text{i}}^{\times}\mathbf{r}_{1,\text{i}} & \mathbf{0}_{3\text{x}1} \\ \mathbf{L}_{3\text{x}6} & \mathbf{0}_{3\text{x}1} & \mathbf{e}_1 \\ \mathbf{L}_{3\text{x}6} & \mathbf{0}_{3\text{x}1} & \mathbf{e}_{2,\text{i}}^{\times}\mathbf{r}_{2,\text{i}} \end{bmatrix}, \tag{10}$$

$$\dot{\boldsymbol{\Theta}} = \begin{bmatrix} \boldsymbol{\omega}_0 \\ \mathbf{v}_{0,\text{i}} \\ \dot{\theta}_1 \\ \dot{\theta}_2 \end{bmatrix} \tag{11}$$

And where $\mathbf{0}_{\text{mxn}}$ is the n-by-m matrix of zeros, and $\mathbf{L}_{\text{mxn}}, n > m$ is the matrix whose left square is the m-by-m identity:

$$\mathbf{L}_{\text{mxn}} = \begin{bmatrix}\mathbf{1}_{\text{mxm}} & \mathbf{0}_{\text{mx(n-m)}}\end{bmatrix} \tag{12}$$

Thus, the NOC matrix $\mathbf{N}$ provides a mapping from the 18D operational space velocities to the 8D joint space velocities which represent the actual system's 8 degrees of freedom. Furthermore, for acceleration mappings, we find by differentiation:

$$\dot{\mathbf{t}} = \mathbf{N}\ddot{\boldsymbol{\Theta}} + \dot{\mathbf{N}}\dot{\boldsymbol{\Theta}} \tag{13}$$

Where:

$$\dot{\mathbf{N}} = \begin{bmatrix} \mathbf{0}_{6x6} & \mathbf{0}_{6x1} & \mathbf{0}_{6x1} \\ \mathbf{0}_{3x6} & \mathbf{0}_{3x6} & \mathbf{0}_{3x1} \\ \mathbf{0}_{3x6} & \mathbf{w}_0^{\times}\mathbf{e}_{1,i}^{\times}\mathbf{r}_{1,i} + \mathbf{e}_{1,i}^{\times}\dot{\mathbf{r}}_{1,i} & \mathbf{0}_{3x1} \\ \mathbf{L}_{3x6} & \mathbf{0}_{3x1} & \mathbf{0}_{3x6} \\ \mathbf{L}_{3x6} & \mathbf{0}_{3x1} & \mathbf{w}_0^{\times}\mathbf{e}_{2,i}^{\times}\mathbf{r}_{2,i} + \mathbf{e}_{1,i}^{\times}\dot{\mathbf{r}}_{2,i} \end{bmatrix} \tag{14}$$

Joint Space Dynamics

Before using the NOC to reduce the dynamic equations, one further note is made, which is that the constraint forces and torques produce no work. The total wrench can be split into two parts:

$$\mathbf{w} = \mathbf{w}_{\mathrm{A}} + \mathbf{w}_{\mathrm{C}} \tag{15}$$

Where $\mathbf{w}_{\mathrm{A}}$ is *active* wrench (the forces and torques from actuators or external disturbances) and $\mathbf{w}_{\mathrm{C}}$ is the constraint wrench (the forces and torques from one body onto another via their couplings). The fact that the constraints produce no work is expressed as:

$$\mathbf{t}^T\mathbf{w}_{\mathrm{C}} = 0 \tag{16}$$

Subbing in Eqn. (9):

$$(\mathbf{N}\dot{\boldsymbol{\Theta}})^T\mathbf{w}_{\mathrm{C}} = 0 \tag{17}$$

And since this holds for all $\dot{\boldsymbol{\Theta}}$:

$$\mathbf{N}^T\mathbf{w}_{\mathrm{C}} = 0 \tag{18}$$

Returning to the system's operational space dynamic equations as given in Eqn. (6), both sides are multiplied by $\mathbf{N}^T$ to find:

$$\mathbf{N}^T\mathbf{M}\dot{\mathbf{t}} + \mathbf{N}^T\mathbf{W}\mathbf{M}\mathbf{t} = \mathbf{N}^T\mathbf{w}_{\mathrm{A}} + \mathbf{N}^T\mathbf{w}_{\mathrm{C}} \tag{19}$$

Using Eqns. (9) and (18) this is reduced to:

$$\mathbf{H}\ddot{\boldsymbol{\Theta}} + \mathbf{C}\dot{\boldsymbol{\Theta}} = \mathbf{T} \tag{20}$$

Where:

$$\begin{aligned} \mathbf{H} &= \mathbf{N}^T\mathbf{M}\mathbf{N}, \\ \mathbf{C} &= \mathbf{N}^T\mathbf{M}\dot{\mathbf{N}} + \mathbf{N}^T\mathbf{W}\mathbf{M}\mathbf{N}, \\ \mathbf{T} &= \mathbf{N}^T\mathbf{w}_{\mathrm{A}} \end{aligned} \tag{21}$$

Eqn (20) and its constituent matrices gives the joint space dynamics. Having models of the active forces and torques, standard integration techniques can be used to solve the forward dynamics in the joint space to describe the multibody spacecraft motion.

III. Guidance, Navigation, and Control Approaches

The GNC system is designed such that the articulation functionality is added onto existing ADCS which has substantial heritage on past single-body SFL spacecraft. Figure 3 gives a high-level overview of the system's architecture in block diagram form. The solid lines in Figure 3 represent components and connections forming the existing single body ADCS loop.

For the sample mission, the main body is equipped with reaction wheels and magnetorquers for attitude actuation, and an attitude sensor suite consisting of Sun sensors, a three axis rate sensor, a magnetometer, and a star tracker which provides a fine level of attitude determination for accurate payload pointing operations. A GPS receiver provides the system with orbit determination along with onboard two-line elements (TLE). Existing flight software running on the spacecraft's onboard computers takes in sensor measurements and begins by performing attitude determination. The attitude estimate is then used along with attitude path planning or guidance to derive an attitude error which is used to inform the control which ultimately generates actuator commands to drive the attitude towards the desired trajectory.

In parallel to the main ADCS loop, the new articulation loop uses hardware consisting of joint motors for actuation and encoders for sensing. Similar to the software in the main loop, the articulation GNC portion of the software takes in sensor measurements and ultimately produces actuator commands. Notably, the objectives of the articulation guidance are generally decoupled from those of the attitude guidance. In other words, while the attitude trajectory may try to point the main body at some target (e.g. a point on the ground), the articulation guidance tries to point the appendages at a separate target (e.g. the Sun).

Sun Tracking

The particular case that will be discussed here is the case where the articulation guidance objective is to track the Sun with the power generating face of a pair of solar arrays, as depicted in Figure 1. In the topology of the sample spacecraft, both joint axes lie on the body X-axis ($\mathbf{e}_1 = \mathbf{e}_2 = [1,0,0]^T$). As stated in section II, by convention the appendage body frames are defined so that a given axis vector is expressed equally in both adjacent body frames, thus the X-axes of the array frames are also along the joint axes. We define the Z-axes of the array frames to point normal to the power generating faces, with the Y-axis completing a right-handed triad. For the two arrays $a = 1, 2$, the articulation angle θ_a is defined as the angle between

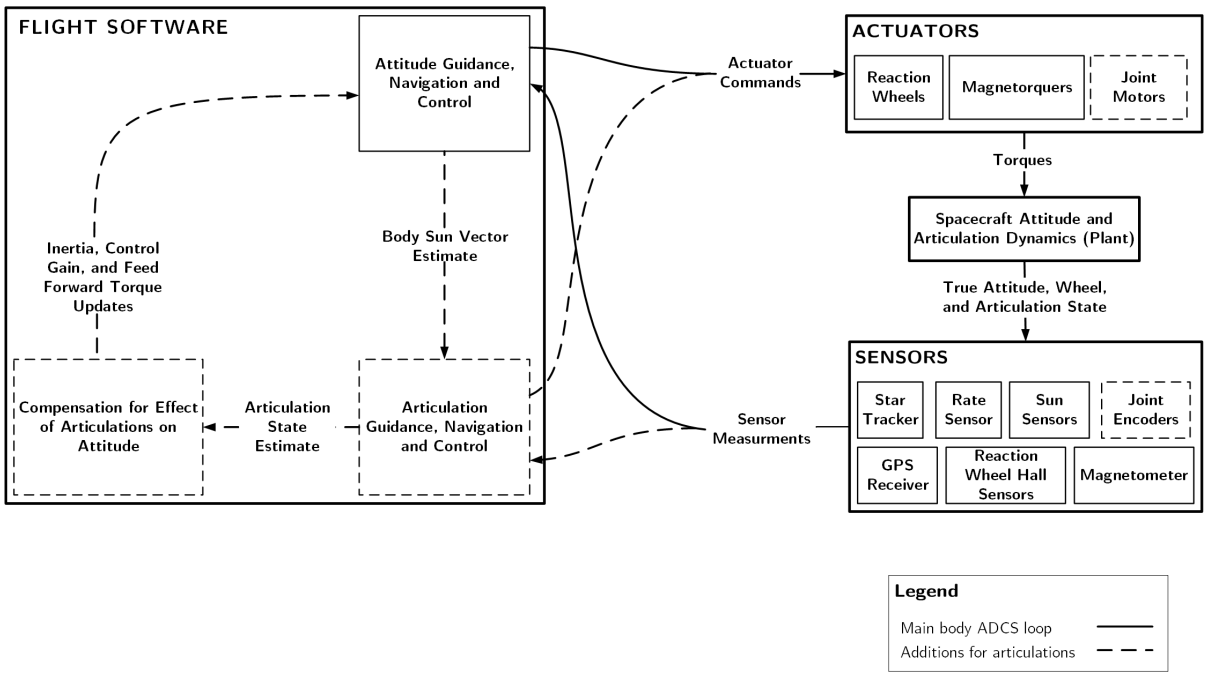

Fig. 3: High-level GNC architecture

$\hat{\underrightarrow{\mathbf{b}}}_3$ and $\hat{\underrightarrow{\mathbf{a}}}_3$ and the body-to-array rotation $\mathbf{C}_{\text{ab}}$ is thus a principle rotation about the X-axis by θ_a:

$$\mathbf{C}_{\text{ab}} = \mathbf{C}_1(\theta_a) = \begin{bmatrix} 1 & 0 & 0 \\ 0 & \cos(\theta_a) & \sin(\theta_a) \\ 0 & -\sin(\theta_a) & \cos(\theta_a) \end{bmatrix} \tag{22}$$

The attitude determination provides an estimate of the body Sun vector $\mathbf{s}_{\text{b,est}}$. This is mapped into the given array frame using that array's rotation estimate ($\theta_{a,est}$):

$$\mathbf{s}_{\text{a,est}} = \mathbf{C}_{\text{ab}}\mathbf{s}_{\text{b,est}} = \begin{bmatrix} s_{b,1} \\ \cos(\theta_{a,est})s_{b,2} + \sin(\theta_{a,est})s_{b,3} \\ -\sin(\theta_{a,est})s_{b,2} + \cos(\theta_{a,est})s_{b,3} \end{bmatrix} \tag{23}$$

The articulation error $\theta_{a,error}$ is then the angle between the normal of the power generating face (in this case the array Z-axis) and the projection of $\mathbf{s}_{\text{a,est}}$ onto the plane which that vector rotates on, (in this case the array YZ-plane). Through some manipulations, the following expression is found:

$$\theta_{a,desired} = \cos^{-1}\left(\frac{\cos(\theta_{a,est})s_{b,3} - \sin(\theta_{a,est})s_{b,2}}{\sqrt{s_{b,2}^2 + s_{b,3}^2}}\right) + \theta_{a,est} \tag{24}$$

Where

$$\theta_{a,error} = \theta_{a,desired} - \theta_{a,est} \tag{25}$$

Note that in general, even with perfect articulation control (i.e., $\theta_{a,error} = 0$ at all times), the array normal may not be perfectly aligned with the Sun due to the Sun being out of the YZ-plane. Due to the single degree of articulation control, the appendages can at best track the projection of a vector onto the plane to which the joint axis is normal. However, the out-of-plane angle can be minimized by defining the attitude trajectory with both objectives in mind. On the sample spacecraft the payload axis (say, the boresight of an imager) is aligned with the body Z-axis. The attitude for payload operations will require that payload to be pointed at some external target. This objective will constrain two degrees of freedom in the attitude, but it will be unconstrained in the third, which is the roll of the main body about the payload axis. To aid in the articulation objective, the roll about the payload axis can be defined to maintain orthogonality between the joint axis and the Sun. To this end, an align-constrain formulation, as described in [9], can be used to set an attitude trajectory that aligns the payload towards its target and constrains the body Y-axis towards the Sun. In this attitude, the Sun inherently lies somewhere on the YZ-plane, and thus, the array normal can be brought in direct alignment with the Sun, subject only to control errors.

Compensation for Effect of Articulation on Attitude

As stated previously, the design employed here leverages heritage ADCS elements for single body spacecraft. The heritage software elements, notably the Extended Kalman Filter (EKF) determination and the control

algorithms rely on the spacecraft being a single rigid body in their usage of a single inertia matrix in dynamic state propagation, gain tuning, and feedforward torque computations. With the addition of the articulating appendages, the inertia of the entire spacecraft now varies as the panels articulate. For these ADCS uses, the inertia is approximated at each timestep by lumping the bodies together at their current positions. Instead of a constant single rigid body inertia $\mathbf{I}_{\mathrm{b}}$, the lumped systems' inertia is used, which is dependant on the time-varying articulation states:

$$\mathbf{I}_{\mathrm{sys}}(\theta_1(t),\theta_2(t)) = \mathbf{J}_{\mathrm{b}}(\theta_1(t),\theta_2(t)) + \mathbf{J}_1(\theta_1(t),\theta_2(t)) + \mathbf{J}_2(\theta_1(t),\theta_2(t)) \quad (26)$$

Where at time t the lumped systems center of mass is computed based on the current articulation state $\mathbf{c}_{\mathrm{sys}}(\theta_1(t),\theta_2(t))$, then $\mathbf{J}_{\mathrm{b}}$, $\mathbf{J}_1$, and $\mathbf{J}_2$ are the main body, and first and second appendage inertias, respectively, expressed about $\mathbf{c}_{\mathrm{sys}}$. Expressions for these component inertias are readily obtained using frame rotations and parallel axis theorem, knowing the constant inertia of each body about its own center of mass and in it's own frame, then using the articulation state and the mechanical geometries to shift and rotate each into a common frame. The updated value of $\mathbf{I}_{\mathrm{sys}}$ at each control cycle can then be used in the EKF state propagation and in order to actively re-tune control gains that are selected based on inertia.

Using only the above inertia update technique to modify the ADCS would not fully address the multibody effects. The system does not in reality become a single body system of inertia $\mathbf{I}_{\mathrm{sys}}$ at each control step, but in reality the appendages move continuously at some velocity inducing some torque on the main body due to coupling dynamics, not to mention the torque of the motors themselves. The coupling or constraint torques can be evaluated using a rearrangement of Eqns. (6, 15) to find $\mathbf{w}_{\mathrm{c}}$. Whereas in section II a joint-space forward dynamics expression was required for the purposes of simulation, here estimates of the velocities and accelerations are used in addition to the active torques based on models of the joint motors and attitude actuators to back out the constraint torques.

IV. Simulation Results

Simulations of the sample mission have been run using SFL's in-house high-fidelity ADCS simulation environment updated to address the multibody dynamics. A $525\,\mathrm{km}$ Sun-synchronous orbit with a 15:00 LTAN was selected as representative for a typical LEO target tracking mission. The spacecraft mass properties and the geometries of the panels and associated linkages are based on a hypothetical DEFIANT structural design. Targets were scattered across the globe, and the mission concept of operations tasks the spacecraft with tracking a given target until it disappears over the horizon, and then rapidly slewing to acquire the next target in its schedule, regardless of whether or not that target is in view. Meanwhile, the attitude Sun constraint and Sun tracking articulation as discussed in section III is implemented.

Figures 4 and 5 show results for the cases where the spacecraft has appendages fixed in place, and where the appendages are articulating to perform Sun tracking, respectively. The top plot of each shows the profile of the spacecraft rate magnitude over a sample time period. The payload is operating as the spacecraft passes over a visible target, and the rate goes up to about $1\,^\circ/\mathrm{s}$ when the target is right below, and slower when it is further off-track. Immediately after a payload operation, the spacecraft slews at a specified rate of $1.5\,^\circ/\mathrm{s}$ to acquire the next target attitude. Slightly more jitter is noted in the rate profile of the articulating case due to the effect of the motor torques and reaction torques and the errors in their compensation. The second plot in each case shows the corresponding payload vector pointing error with respect to the true desired trajectory. There are large spikes in error when the high rate transition slews occur, but those errors settle out well before another payload operation needs to occur and are thus not of concern. During payload operations the error generally stays below $0.5\,^\circ$ in the fixed appendage case, and $0.6\,^\circ$ in the articulating case, spiking up to at worst $1.2\,^\circ$ or $1.4\,^\circ$ in each. As with the rate profile, we note qualitatively the presence of some additional jitter in the motion. The 2σ payload pointing error during all payload operations periods over a $24\,\mathrm{hr}$ simulation is found to be $0.55\,^\circ$ in the fixed appendage case and $0.62\,^\circ$ in the articulating case. Although the targets in the period shown are spaced by about $15-20\,\mathrm{min}$, there is no reason they can't be placed closer together, down to about $3\,\mathrm{min}$ apart to allow for the slew and settling.

Figure 6 shows the results associated with the articulation during the same time period, for one of the two appendages (the results are virtually identical between the two). A desired trajectory is set in order to minimize the angle from the power generating surface to the Sun as described in section III. The sample mission spacecraft uses a stepper motor for the articulation actuation and is only actuated on discrete increments of $4\,^\circ$ in articulation error. The callout box which zooms in on a small time region shows this behaviour with respect to the smooth desired Sun-tracking trajectory. Aside from this behaviour, the trajectory is well followed.

The second plot in Figure 6 shows the control error and angle between the solar array normal and the Sun.

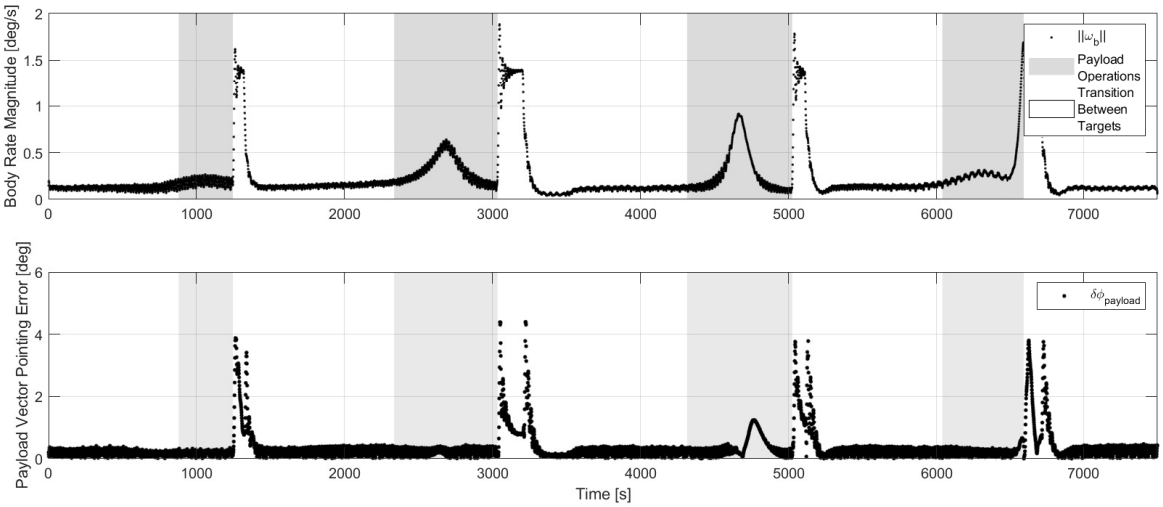

Fig. 4: Simulated body rate magnitude and pointing error during operations *with appendages fixed*

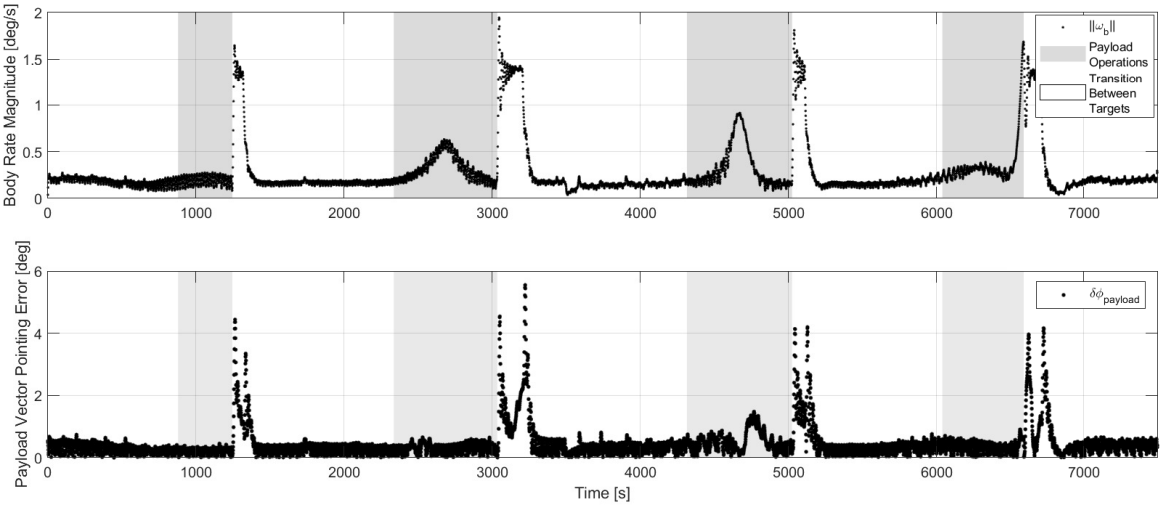

Fig. 5: Simulated body rate magnitude and pointing error during operations *with Sun-tracking articulation enabled*

For the most part, due to the Sun-constrained attitude that brings the Sun within the plane to which the joint axis is normal, the two quantities are the same. It is only the articulation control error that contributes to the $\theta_{array-to-Sun}$ angle because the out-of-plane errors are near zero. We see the control error profile primarily consists of the repeating 4° increments as discussed above. Periodically, however, $\theta_{array-to-Sun}$ grows much larger and drifts away from the θ_{error} term. These instances are during the transition slews between targets. Whereas during the payload operations periods, the main body Y-axis-to-Sun constraint is being adhered to by the attitude guidance, during these transition slews no such constraint is used, and the attitude is governed by an optimal slew maneuver between initial and final states [10]. Because of this, the Sun drifts out of the YZ-plane, and even though the control is still keeping the angle to the Sun projection low, the actual angle to Sun grows larger. These slew periods are quite short overall (generally about $180\,\mathrm{s}$ or less), and therefore have minimal impact on the whole orbit power generation.

Figure 7 shows power generation characteristics over a longer period of operations of $24\,\mathrm{hrs}$. The top plot shows the power generation coefficient $0 \leqslant \gamma \leqslant 1$, which depends on the solar incident angle β according to the Kelly Cosine [11], and which relates the actual generated power $P_{gen}(\beta)$ to the max power that is generated at zero incident angle $P_{max} = P_{gen}(0)$:

$$P_{gen}(\beta) = \gamma(\beta) P_{max} \tag{27}$$

It is apparent that the articulation control keeps the power generation coefficient very near 1 overall, with

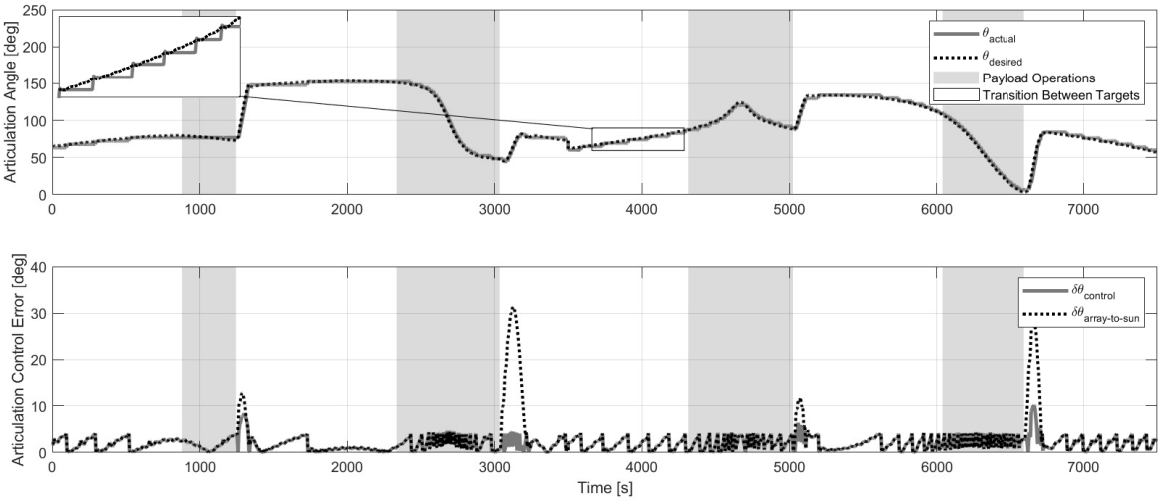

Fig. 6: Sun tracking appendage articulation angle compared to desired trajectory and articulation control errors during operations; callout box highlights stepping profile

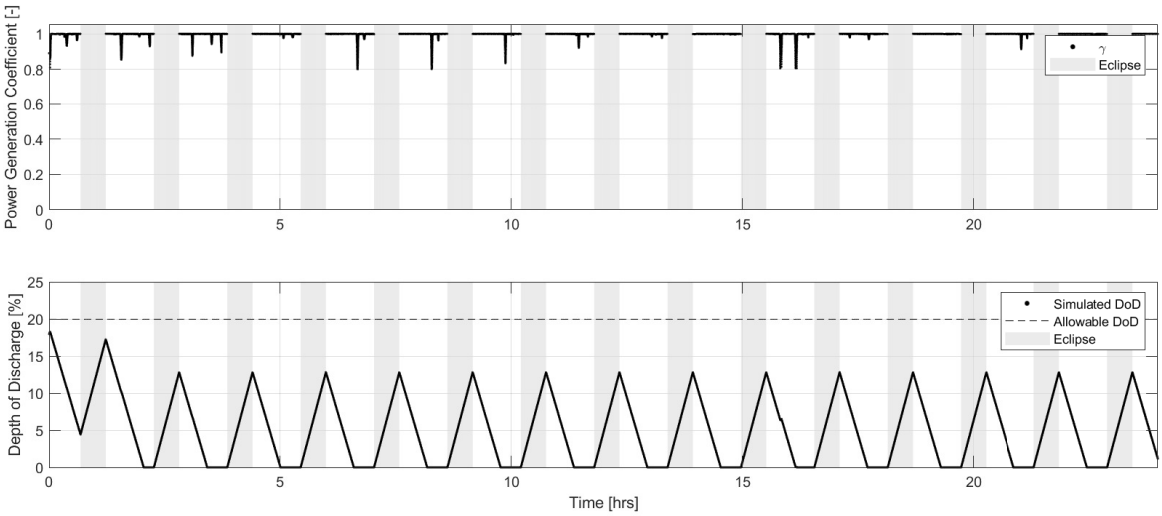

Fig. 7: Solar array power generation coefficient and battery depth-of-discharge over 24hr simulation

the notable dips that occur during slews for reasons discussed above. The second plot in Figure 7 shows battery depth-of-discharge. For this, we assume a continuous bus power consumption of $50\,\mathrm{W}$, a battery with capacity of $200\,\mathrm{W\,h}$, and power generation based on arrays each with five strings of standard satellite solar cells. We initialize the battery at a depth-of-discharge of 18% and set an allowable limit of 20% beyond which the battery performance may be impacted. During the first sunlit period the depth-of-discharge drops from 18% to 5%, and by the next sunlit period it reaches full charge. During each eclipse the depth-of-discharge grows linearly due to zero power generation, but then back in sunlight the high generation reliably drops it to zero well before the next eclipse period is reached.

V. Conclusion

The multibody dynamics governing small spacecraft with articulating arrays have been outlined in the paper. In addition, GNC considerations for achieving decoupled payload and array tracking objectives have been presented. A sample mission using SFL's DEFIANT bus with two deployable articulating arrays has been used to validate the GNC design. Results from simulation indicate that pointing error of $0.62\,^\circ$, 2σ can be achieved during payload operations with concurrent articulation, in comparison with $0.55\,^\circ$, 2σ error for the equivalent fixed, single body case. For the vast majority of practical cases this $0.07\,^\circ$ increase would be of little consequence, and likely it could be further reduce through controller optimization. The Sun-tracking articulation tracks the

Sun sufficiently to maintain a high power generation coefficient throughout operations. This technology thus enables a new class of mission demanding high power generation for payloads with high consumption and operational duty cycle.

ACKNOWLEDGMENTS

The author would like to thank the co-authors Dr. Robert E. Zee, Brad Cotten and Niels Roth for their feedback and collaboration on this research project. In addition, Robin Aucoin is owed thanks for his thorough review of this paper. Finally, the author would like to acknowledge those involved in other intersecting aspects of the deployable and articulating solar array project, including: Mayes Mullins, Suraj Sridharan, Payam Mehradnia, Rami Kandela, and others.

REFERENCES

[1] J. Angeles and S. K. Lee, "The formulation of dynamical equations of holonomic mechanical systems using a natural orthogonal complement," *Journal of applied mechanics*, vol. 55, p. 243, 1988.

[2] J. Angeles and O. Ma, "Dynamic simulation of n-axis serial robotic manipulators using a natural orthogonal complement," *The International Journal of Robotics Research*, vol. 7, no. 5, pp. 32–47, 1988.

[3] S. K. Saha and J. Angeles, "Dynamics of nonholonomic mechanical systems using a natural orthogonal complement," 1991.

[4] S. K. Saha, "Dynamics of serial multibody systems using the decoupled natural orthogonal complement matrices," *Journal of applied mechanics*, vol. 66, no. 4, pp. 986–996, 1999.

[5] J. Virgili-Llop, D. Drew, M. Romano, G. V. Hobson, B. E. Wakefield, and W. B. Roberts, "Spacecraft robotics toolkit: An open-source simulator for spacecraft robotic arm dynamic modeling and control.," in *6th International Conference on Astrodynamics Tools and Techniques*, 2016.

[6] C. Rui, I. V. Kolmanovsky, and N. H. McClamroch, "Nonlinear attitude and shape control of spacecraft with articulated appendages and reaction wheels," *IEEE Transactions on Automatic Control*, vol. 45, no. 8, pp. 1455–1469, 2000.

[7] "SFL satellite platforms." https://www.utias-sfl.net/?page_id=89. Accessed: 2020-05-20.

[8] A. H. de Ruiter, C. Damaren, and J. R. Forbes., *Spacecraft Dynamics and Control: An Introduction*. John Wiley & Sons, Ltd, 2013.

[9] R. D. Magner, "Extending target tracking capabilities through trajectory and momentum setpoint optimization," *AIAA/USU Conference on Small Satellites*, 2018.

[10] R. Aucoin, "Real-time optimal slew maneuver planning for small satellites," *AIAA/USU Conference on Small Satellites*, 2019.

[11] M. R. Patel, *Spacecraft power systems*. CRC press, 2004.